Received 27 February 2024; revised 17 April 2024; accepted 22 April 2024. Date of publication 3 May 2024; date of current version 6 August 2024.

Digital Object Identifier 10.1109/OJAP.2024.3396501

Refinements to the Design of Traveling-Wave Waveguide Slot Arrays

JACOB C. COETZEE (Senior Member, IEEE)

School of Electrical Engineering and Robotics, Queensland University of Technology, Brisbane, QLD 4001, Australia

CORRESPONDING AUTHOR: J. C. COETZEE (e-mail: jacob.coetzee@qut.edu.au)

ABSTRACT A traveling-wave array of longitudinal slots in the broad wall of a waveguide offers greater impedance bandwidth compared to standing-wave slot arrays. Narrow-beam applications typically require a main beam at a chosen off-broadside direction and low sidelobes in other directions. Since a portion of the input power is dissipated in a load, wideband performance is achieved at the expense of reduced radiation efficiency. Without compensation for the effects of the array element radiation pattern, conventional array synthesis approaches produce sidelobe levels that do not meet the original specification. Existing remedial design techniques use optimization to address either sidelobe performance, impedance bandwidth or efficiency. This paper presents a new design approach that not only ensures that sidelobes specifications are met, but also achieves good impedance matching and high efficiency. The procedure is demonstrated using a 21-element array in standard X-band waveguide and performance is validated though both simulation and measurement.

INDEX TERMS Waveguide, antenna arrays, radar antennas, slot antennas, traveling-wave, antenna radiation patterns.

I. INTRODUCTION

WAVEGUIDE slot arrays are widely used in radar and remote sensing applications [1]. These arrays are predominantly implemented in standing wave configuration; however traveling-wave arrays offer some advantages [2]. They have off-broadside main beams and feature greater impedance bandwidth, albeit at the expense of reduced radiation efficiency. One of the design objectives for traveling-wave arrays is to have low-sidelobe radiation patterns, but practical implementations often do not meet the intended side-lobe level specification [3]. Without proper consideration of element spacing, they can also produce radiation patterns with unwanted grating lobes.

Other researchers have reported improved performance of traveling-wave slot arrays. One approach involves the application of a full-wave finite element or method of moment analysis to an existing design and performing optimization by perturbing the slot dimensions to improve the array performance [4], [5], [6]. This optimization process involves repeated application of a full-wave analysis of the array, which can be cumbersome and very time consuming. It also requires access to custom analysis code or commercial software. Apart from radiation characteristics, traveling-wave slot arrays also have other important performance metrics. The array is required to present an impedance match over a range of frequencies. Since one end of the array is terminated in a matched load that dissipates a portion of the input power, the array's efficiency is also an important consideration. In the approach presented in [4], optimization is carried out with the focus on either sidelobe performance, impedance matching or efficiency.

In this paper, a new systematic design approach is presented. Specific guidelines for the determination the element spacing are provided. The clear need for accommodating the effects of the element pattern in the determination of the array element excitation coefficients is demonstrated. During the first step of the proposed design procedure, element excitations are adjusted to ensure that the SLL specifications are met. The second step involves the calculation of the slot dimensions. The fundamental design equations used during this step are similar to those of [3], [5], but due to the reduced element spacing in traveling-wave arrays, additional compensation for higher-order internal coupling is incorporated in the expression for the active

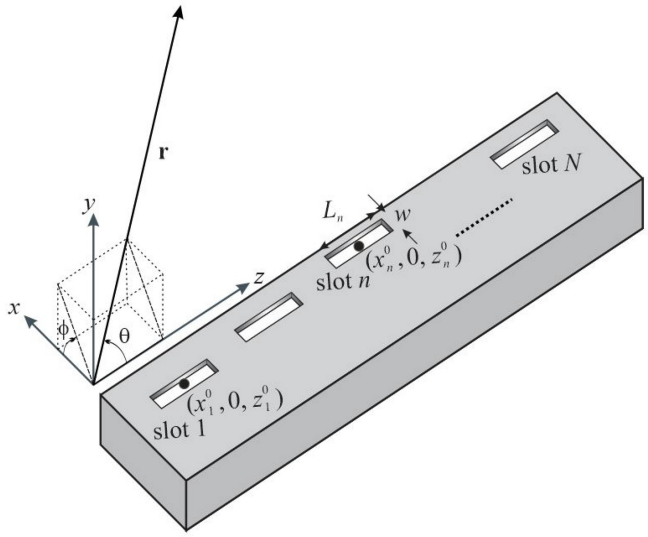

FIGURE 1. Geometry of a linear array of *N* slots.

admittance of each slot. The design criteria are combined in such manner as to ensure that the performance criteria of sidelobe performance, impedance matching and efficiency are addressed simultaneously. The method is efficient and offers superior performance to existing formulations. The procedure is demonstrated using the design example described in [3].

II. DESIGN PARAMETERS

Consider a linear array of longitudinal slots in the broad wall of a rectangular waveguide, as illustrated in Fig. 1. The total number of slots in the array is N and each slot has a width w. Slot n is centered at the point $(x_n^0, 0, z_n^0)$. Its excitation is determined by the length L_n and offset from the centerline of the waveguide, x_n^{off}. Radiation is typically observed in the far zone with the direction defined by angles θ and ϕ, with $\theta = \phi = 90°$ representing the broadside direction and the plane $\phi = 90°$, $0° \le \theta \le 180°$ being H-plane of the array.

A. ELEMENT SPACING

The two main criteria for implementing a narrow-beam traveling wave array are to have a main beam located at a specific angle of $\theta = \theta_0$ while having sidelobes at $-R_0$ dB relative to the main beam. Conventional design techniques for broadside arrays often use Chebyshev excitations $|c_n|$ to satisfy the desired sidelobe specification. To direct the main beam to the pointing angle θ_0, the required phase progression ψ between adjacent slots is calculated using

$$\psi = -k_0 d \cos\theta_0 \tag{1}$$

where k_0 is the free space wave number at the design frequency and d is the slot spacing. The phase-adjusted slot excitations can then be defined as

$$c_n = |c_n| e^{j(n-1)\psi}. \tag{2}$$

The design of traveling wave arrays allows for some flexibility in selecting the squint angle at the design frequency. The choice of angle that results in near-resonant slots is

$$\theta_0 \approx \cos^{-1} \frac{\beta_{10}}{k_0} \tag{3}$$

with β_{10} being the TE_{10} mode phase constant. A different choice of θ_0 will require non-resonant slots in order to meet the phase requirements of the element excitations specified in (2). The next design consideration is the choice of inter-element spacing. We calculate the normalization parameter z_0 from [7]

$$z_0 = \cosh \frac{\cosh^{-1} 10^{R_0/20}}{N-1}. \tag{4}$$

For a Chebyshev array with maximum radiation at broadside (i.e., $\theta_0 = 90°$), suppression of array factor minor lobes imposes a limit on the maximum element spacing of [7]

$$d_{\max}/\lambda_0 = \cos^{-1}(-1/z_0)/\pi \tag{5}$$

where λ_0 is the free space wavelength. In the general case where $\theta_0 < 90°$, (5) is adapted to

$$d_{\max}/\lambda_0 = \frac{\cos^{-1}(-1/z_0)}{\pi(1 + |\cos\theta_0|)}. \tag{6}$$

A suitable value for the slot spacing is thus $d \le d_{\max}$. A choice of slot spacing that exceeds $d_{\max}$ will result in the emergence of a grating major lobe in the visible region.

The relationship between the maximum slot spacing, squint angle, sidelobe level (SSL) requirement and the size of the array is depicted in Fig. 2. For squint angles $\theta_0 < 90°$, the offset polarity for all slots will be identical. In an array environment, the typical resonant slot length is $L \approx 0.48\lambda_0$. Slot lengths of a traveling-wave array vary, but a realistic upper limit would be approximately $0.5\lambda_0$. Due to potential overlapping between adjacent slots, solutions within the shaded area in Fig. 2 may not be viable. For squint angles closer to broadside, the maximum element spacing is more relaxed and gradually becomes more restrictive as θ_0 deviates further away from 90°. For a fixed value of θ_0, lower sidelobes (i.e., increasing R_0) require more closely-spaced elements. With fixed values of R_0 and θ_0, an array with a large number of elements tolerates larger element spacing compared to an array with fewer elements.

The array factor for a broadside Checyshev array of order N in the H-plane is given by [7]

$$AF(\theta) = T_{N-1}(z_0 u) \tag{7}$$

where $T_m(x)$ is the mth order Chebyshev polynomial and $u = \pi(d/\lambda_0)\cos\theta$. With element excitations adjusted to produce a main beam at $\theta = \theta_0$, the array factor can be expressed as

$$AF(\theta) = T_{N-1}[z_0(u - u_0)] \tag{8}$$

with $u_0 = \pi(d/\lambda_0)\cos\theta_0$. The example in [3] comprises an array of 21 slots in standard WR90 waveguide (width $a = 22.86$ mm, $b = 10.16$ mm) with a squint angle of

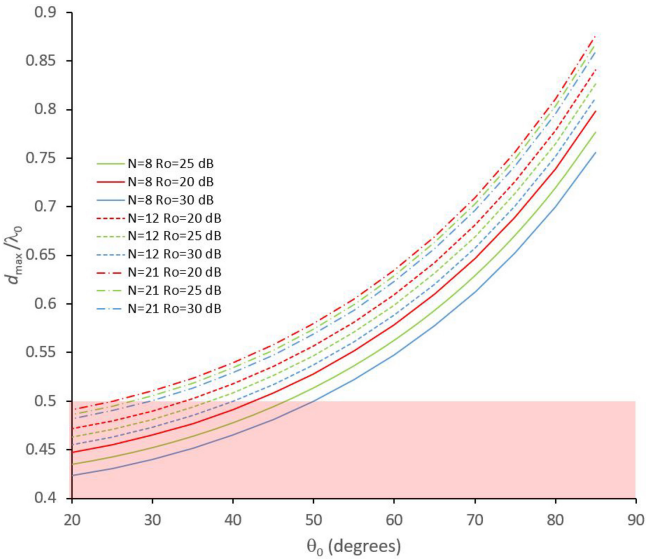

FIGURE 2. Maximum element spacing as a function of the squint angle for different values of the required SSL R_0 and the number of array elements N.

TABLE 1. Parameters for design example.

Quantity	Symbol	Value
free space wave number	k_0	196.486 rad/m
TE_{10} mode phase constant	β_{10}	140.429 rad/m
free space wavelength	λ_0	31.978 mm
guide wavelength	λ_{10}	44.743 mm
normalization parameter	z_0	1.0216
maximum normalized slot spacing	$d_{\max}/\lambda_0$	0.5474

$\theta_0 = 45°$ and a target of -30 dB sidelobes at a frequency 9.375 GHz. The relevant parameters for this example are listed in Table 1. Fig. 3(a) shows the normalized array factor $AF_{\rm n}(\theta) = AF(\theta)/AF(\theta_0)$ of the 21-element array with phase-adjusted Chebyshev excitation coefficients and a slot spacing $d = 0.54\lambda_0$. Since $d < d_{\max}$, the array factor shows a single main lobe at $\theta_0 = 45°$ with no grating lobe. In Fig. 3(b), the slot spacing of $d = 0.55\lambda_0$ marginally exceeds the maximum, and the emergence of a grating lobe becomes evident. With a slot spacing of $d = 0.6\lambda_0$ in Fig. 3(c), the grating lobe is fully developed to form an unwanted second major lobe.

B. COMPENSATION FOR EFFECTS OF THE ELEMENT PATTERN

Consider a single slot of length L and width w, as depicted in Fig. 4. By assuming a piecewise sinusoidal aperture field distribution, utilizing the expression for radiated fields from a finite length electric dipole [7] and applying the duality theorem, the normalized far-field radiation pattern of the slot element can be calculated as

$$E_\phi^{\rm slot}(\theta,\phi) = \operatorname{sinc}(k_0 \sin\theta\cos\phi\, w/2) \times \frac{\cos(k_0\cos\theta\, L/2) - \cos(k_0 L/2)}{\left[1-\cos(k_0 L/2)\right]\sin\theta}. \quad (9)$$

Note that the radial dependence of $\exp(-jk_0 r)/r$ has been suppressed in (9).

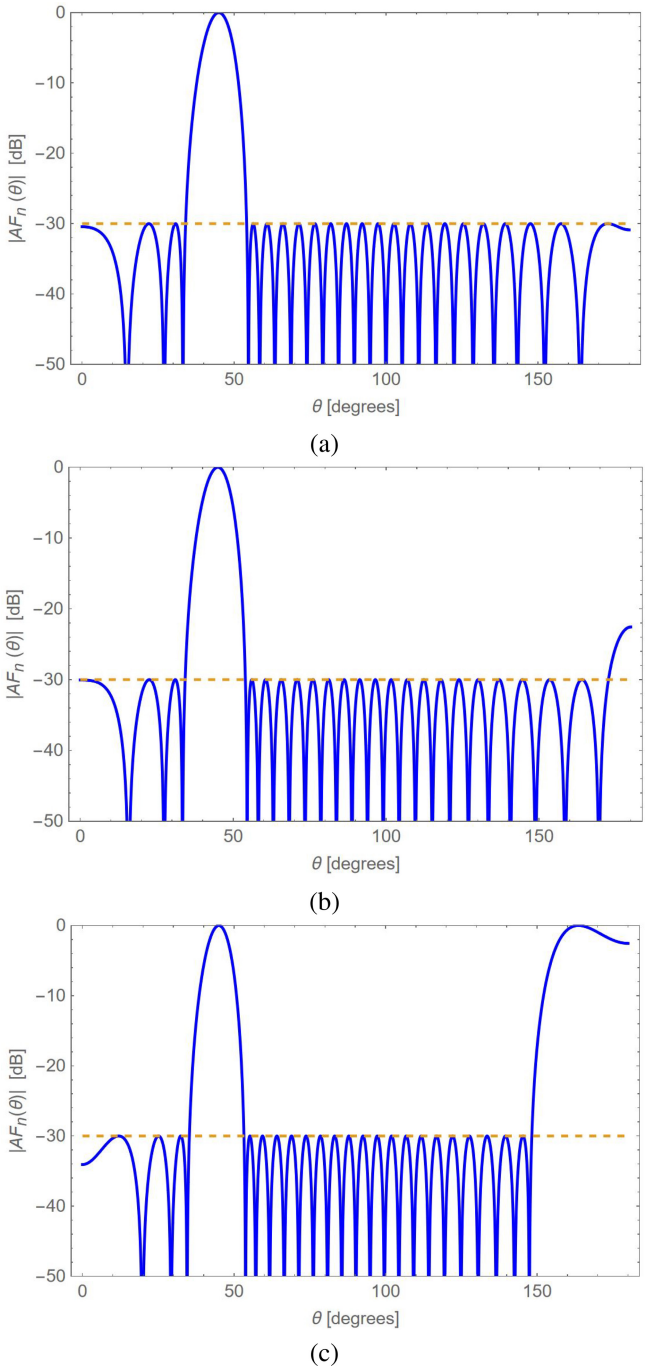

FIGURE 3. Normalized array factor of a 21-element Chebeyshev array with an SSL of -30 dB, a squint angle of $\theta_0 = 45°$ and an element spacing of (a) $d = 0.54\lambda_0$, (b) $d = 0.55\lambda_0$, and (c) $d = 0.6\lambda_0$.

The radiated far-field of a linear or planar array of N slots can thus in general be expressed as

$$E_\phi(\theta,\phi) = \sum_{n=1}^{N} c_n \exp\left[jk_0\left(x_n^0\sin\theta\cos\phi + z_n^0\cos\theta\right)\right] \times \operatorname{sinc}(k_0\sin\theta\cos\phi\, w/2) \times \times \frac{\cos(k_0\cos\theta\, L_n/2) - \cos(k_0 L_n/2)}{[1-\cos(k_0 L_n/2)]\sin(k_0 L_n/2)\sin\theta}. \quad (10)$$

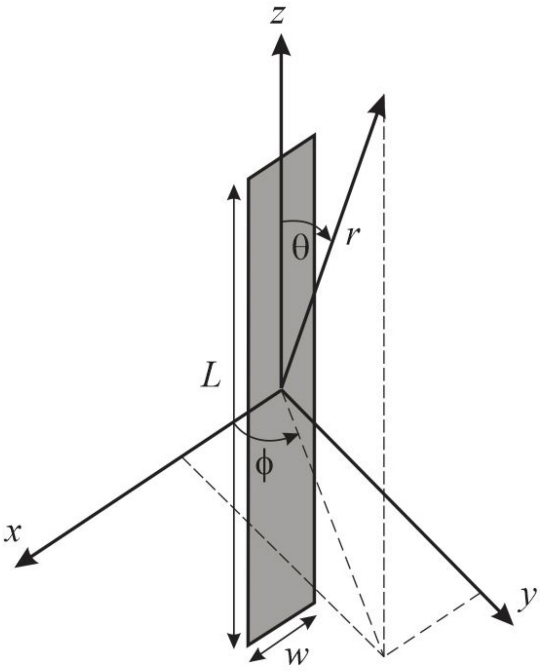

FIGURE 4. A longitudinal slot centered at the coordinate system origin.

Since the slots of an array do not have uniform lengths, the expression for the total field in (10) can strictly not be expressed as the product of the array factor and an element pattern. However, if the variation in slot length is limited, an average slot length L_{av} can be utilized to yield an approximate uniform element pattern. In the H-plane, the array factor of a linear array of equally-spaced slots becomes

$$AF(\theta) = \sum_{n=1}^{N} c_n \exp\left[j2\pi(n-1)(d/\lambda_0)\cos\theta\right]. \tag{11}$$

With phase-adjusted Chebyshev coefficients as in (2), the expressions in (11) and (8) produce identical normalized patterns. The approximate element pattern in the H-plane can be expressed as

$$EP(\theta) = \frac{\cos(\cos\theta\,\pi L_{\text{av}}/\lambda_0) - \cos(\pi L_{\text{av}}/\lambda_0)}{\left[1-\cos(\pi L_{\text{av}}/\lambda_0)\right]\sin\theta}. \tag{12}$$

The total field becomes

$$TF(\theta) = AF(\theta) \times EP(\theta) \tag{13}$$

or, in normalized form,

$$TF_{\text{n}}(\theta) = \frac{AF(\theta)}{AF(\theta_0)} \times \frac{EP(\theta)}{EP(\theta_0)}. \tag{14}$$

Calculations were performed for our design example with a slot spacing of $d = 0.544\lambda_0$ and a realistic average slot length of $L_{\text{av}} = 0.485\lambda_0$. The array factor shown in Fig. 5(a) uses phase-adjusted Chebyshev excitations and meets the sidelobe specification of −30 dB. As expected, it produces a main beam at $\theta_0 = 45°$, and since $d < d_{\max}$, there is no grating lobe. The element pattern in Fig. 5(a) has a maximum at $\theta = 90°$ and nulls at $\theta = 0°$ and $\theta = 180°$. Fig. 5(b) shows the product of the radiation patterns of Fig. 5(a). Due to the fact that $EP(\theta_0) < 0$, the main lobe is suppressed and the sidelobes are no longer of uniform amplitude. The sidelobes of the normalized total field in Fig. 5(c) become elevated in the angular sector around broadside and the total field no longer meets the sidelobe specification.

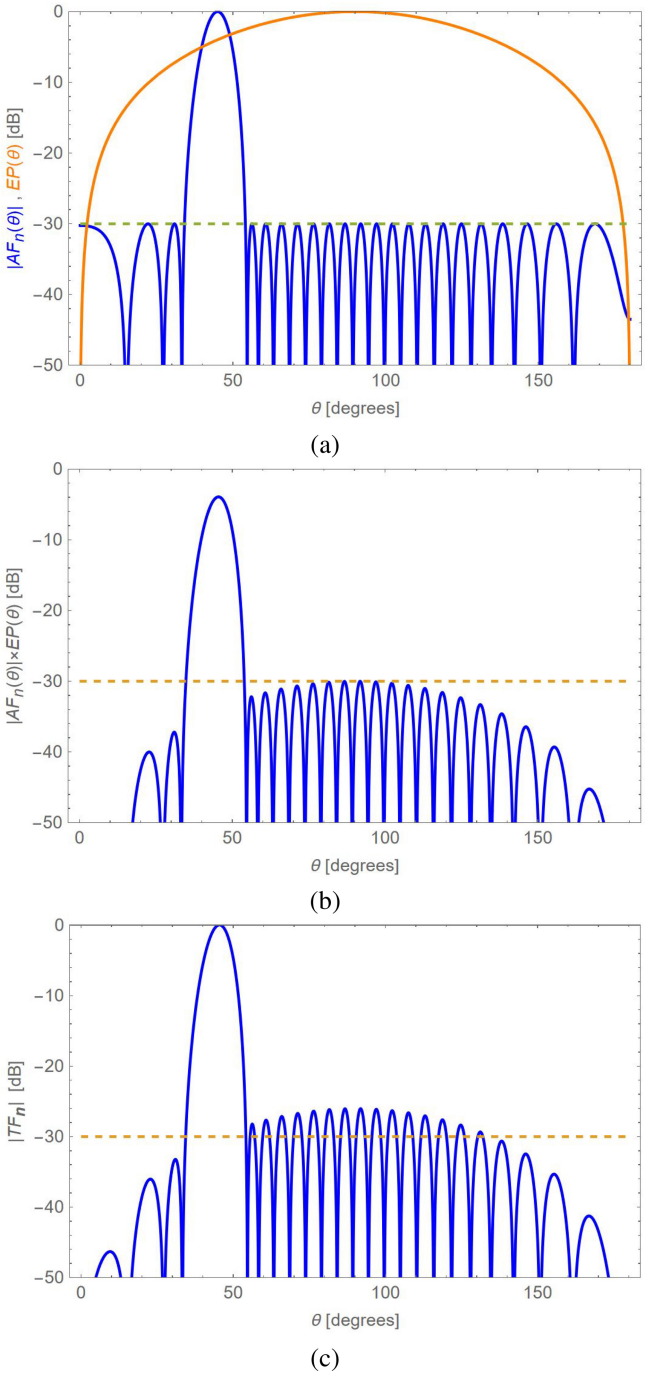

FIGURE 5. (a) Normalized array factor and element pattern, (b) product of normalized array factor and element pattern and (c) normalized total field of the 21-element Chebeyshev array.

This effect applies to all traveling-wave slot arrays and becomes more severe with greater deviation of the quint angle from broadside. It explains the inability to achieve the desired sidelobe performance of the example presented in [3]. The author ascribed the performance deficiency to internal mutual coupling that was not accounted for, but it can be argued that the main cause was neglecting the effects of the element pattern in determination of the element excitations.

Improved performance of traveling-wave slot arrays have been reported [4], [6]. The method involves a procedure where the array is repeatedly analyzed and slot dimensions are adjusted until the performance goal is reached. The optimization variables are the slot dimensions.

A new approach for addressing this issue is proposed. Instead of optimizing the slot dimensions to achieve the desired radiation pattern, we adjust the amplitude of the excitation coefficients. During each step of the optimization, the locations of the sidelobe maxima $\theta = \theta_i, i = 1, 2, \ldots, I$ are determined by numerically evaluating and solving the relation

$$\frac{\partial}{\partial\theta}\left|TF_{\mathrm{n}}(\theta_i)\right| = 0 \tag{15}$$

where $\frac{\partial^2}{\partial\theta^2}|TF_{\mathrm{n}}(\theta_i)| < 0$ and $\theta \neq \theta_0$. The sidelobes at locations $\theta = \theta_j, j = 1, 2, \ldots, J$ that exceed the sidelobe specification (i.e., where $20\log|TF_{\mathrm{n}}(\theta_j)| > -R_0$) are identified. The cost function is evaluated as

$$f_a = \sum_{j=1}^{J} R_0 + 20\log|TF_{\mathrm{n}}(\theta_j)|. \tag{16}$$

A suitable optimization procedure is employed to minimize (16) with the amplitude of slot excitations $|c_n|$ as variables and the original Chebyshev coefficients as initial guesses. The solution ensures that the sidelobe specification is met or exceeded for each of the minor lobes.

Table 2 shows the original Chebyshev coefficients and the adjusted element excitations for the 21-element design example with −30 dB sidelobes. While the original Chebyshev coefficients are symmetrical, a minor degree of asymmetry for the modified element exitations is evident. Also note that the modified excitation requires additional amplitude tapering, but in light of the reduced sidelobes, this is to be expected. The total field was recalculated and is shown in Fig. 6. Although it is not possible to synthesize a pattern with uniform sidelobes, the pattern meets the requirement of having all sidelobes at or below the required maximum.

III. ARRAY DESIGN

The design method is similar to the method described in [3], but with some subtle variations to ensure that performance criteria related to radiation characteristics, impedance matching and efficiency are addressed simultaneously.

A. DESIGN EQUATIONS

The equivalent circuit of an N-element array is shown in Fig. 7. It consists of N shunt elements separated by

TABLE 2. Original Chebyshev coefficients and modified element excitations.

n	1	2	3	4	5	6	7
$\lvert c_n\rvert$ (original)	0.334	0.279	0.378	0.485	0.595	0.701	0.800
$\lvert c_n\rvert$ (modified)	0.219	0.234	0.334	0.439	0.556	0.668	0.775
n	8	9	10	11	12	13	14
$\lvert c_n\rvert$ (original)	0.883	0.947	0.986	1.000	0.986	0.947	0.883
$\lvert c_n\rvert$ (modified)	0.870	0.937	0.987	1.000	0.983	0.939	0.868
n	15	16	17	18	19	20	21
$\lvert c_n\rvert$ (original)	0.800	0.701	0.595	0.485	0.378	0.279	0.334
$\lvert c_n\rvert$ (modified)	0.777	0.670	0.551	0.439	0.332	0.242	0.217

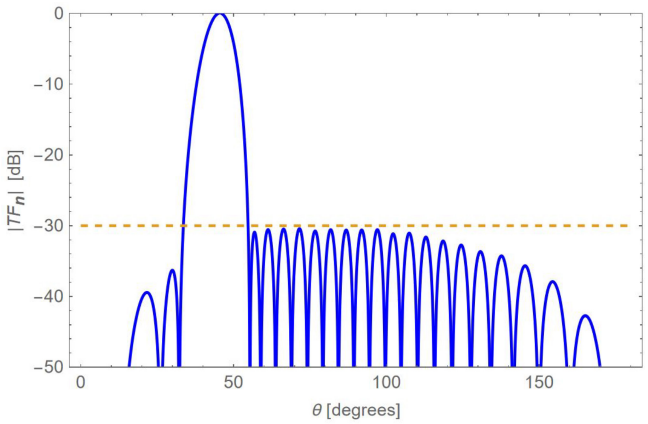

FIGURE 6. Total field of the 21-element array with modified element exitations.

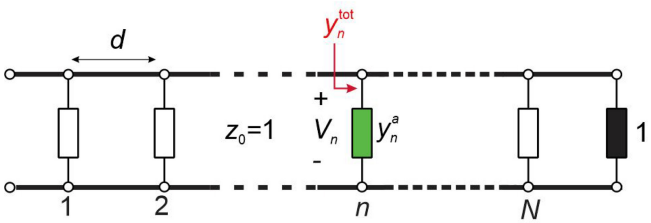

FIGURE 7. Equivalent circuit of an *N*-element traveling-wave slot array with element spacing *d* and terminated in a matched load.

sections of transmission line and where $y_n^a = g_n^a + jb_n^a$ represents the normalized active admittance of slot n. The voltage across y_n^a is denoted as V_n and the slot voltage at the center of the slot is V_n^{slot}. We use a normalized characteristic impedance $z_0 = 1$ in all calculations involving the equivalent circuit.

Elliott's first design equation [8] establishes a relationship between y_n^a, V_n^{slot} and V_n. It is given by

$$y_n^a = K_1 f_n \frac{V_n^{\mathrm{slot}}}{V_n}. \tag{17}$$

The constant K_1 and the term f_n are given in [9].

The second design equation provides an expression for the active admittance in terms of the admittance of the isolated slot, y_n^{self}, and three other terms which account for

external and higher-order internal mutual coupling between the radiating elements. It is given by

$$\frac{1}{y_n^a} = \frac{1}{y_n^{\text{self}}} + \frac{1}{K_2 f_n^2} \sum_{\substack{m=1 \\ m\neq n}}^{N} \frac{V_m^{\text{slot}}}{V_n^{\text{slot}}} g_{mn} + \frac{1}{K_3 f_n^2} \frac{V_{n-1}^{\text{slot}}}{V_n^{\text{slot}}} h_n^{20} h_{n-1}^{20} + \frac{V_{n+1}^{\text{slot}}}{V_n^{\text{slot}}} h_n^{20} h_{n+1}^{20} + \frac{1}{K_6 f_n^2} \frac{V_{n-1}^{\text{slot}}}{V_n^{\text{slot}}} h_n^{01} h_{n-}^{01} + \frac{V_{n+1}^{\text{slot}}}{V_n^{\text{slot}}} h_n^{01} h_{n+1}^{01} \tag{18}$$

with the terms K_2, K_3, K_6, g_{mn}, h_n^{20} and h_n^{01} as defined in [9], [10] and [11]. Compensation for higher-order mode internal coupling between slots of resonant slot arrays only accommodates the TE_{20} mode [12]. However, with the reduced element spacing for traveling-wave arrays, TE_{01} mode coupling between slots can also be significant and was therefore included in (18). The slot voltages are set equal to the complex element excitation coefficients, i.e., $V_n^{\text{slot}} = c_n,\ n = 1, 2, \ldots, N$.

With reference to Fig. 7, the total admittance seen from the nth shunt element looking toward the loaded end of the circuit is given by

$$y_n^{\text{tot}} = \begin{cases} y_n^a + 1 & n = N \\ y_n^a + \dfrac{y_{n+1}^{\text{tot}} \cos(\beta_{10} d) + j \sin(\beta_{10} d)}{\cos(\beta_{10} d) + j y_{n+1}^{\text{tot}} \sin(\beta_{10} d)} & n < N. \end{cases} \tag{19}$$

The voltage ratio (V_n/V_1) can thus be computed as

$$(V_n/V_1) = \frac{(V_{n-1}/V_1)}{\cos(\beta_{10} d) + j y_n^{\text{tot}} \sin(\beta_{10} d)} \qquad n = 2, 3, \ldots, N. \tag{20}$$

From (17), we obtain the relation

$$\frac{V_n^{\text{slot}}}{V_1^{\text{slot}}} = \frac{y_n^a f_1 (V_n/V_1)}{y_1^a f_n} \tag{21}$$

with y_n^a as defined in (18).

The normalized input admittance of the array as seen from the first slot is given by

$$y_{\text{in}} = g_{\text{in}} + j b_{\text{in}} = y_1^{\text{tot}}. \tag{22}$$

The corresponding reflection coefficient at the input is thus

$$\Gamma_{\text{in}} = \frac{1 - y_{\text{in}}}{1 + y_{\text{in}}}. \tag{23}$$

An impedance match at the input would be achieved when $\Gamma_{\text{in}} = 0$.

The fraction of the power absorbed in the matched load relative to the total power accepted at the input of the array can be calculated from

$$P_{\text{L}}/P_{\text{in}} = |V_N/V_1|^2 / g_{\text{in}}. \tag{24}$$

According to (2), the element excitations V_n^{slot} and V_{n-1}^{slot} should have a fixed phase difference of ψ radians. Admittances y_n^{tot} are generally complex-valued, and inspection of (20) shows that the phase difference between voltages V_n and V_{n-1} varies for different values of index n. The phase discrepancy needs to be offset by complementary phase differences between y_n^a and y_{n-1}^a. This implies that for a traveling-wave array with uniform element spacing, only one of the slots can be resonant, unlike resonant slot arrays where all slots are resonant. Resonance of slot n can be achieved by enforcing the requirement that $b_n^a = 0$.

B. DESIGN PROCEDURE

To account for the effects of internal and external mutual coupling, an iterative design approach is employed to determine the length and offset for each of the slots, similar to the method described in [8]. In contrast to solving a set of nonlinear equations during each iteration, we instead employ an optimization procedure to minimize a cost function

$$f_b = w_1 \sum_{n=2}^{N} \left| \frac{V_n^{\text{slot}}}{V_1^{\text{slot}}} - \frac{y_n^a f_1 (V_n/V_1)}{y_1^a f_n} \right|^2 + w_2 |\Gamma_{\text{in}}|^2 + w_3 (P_{\text{L}}/P_{\text{in}})^2 + w_4 |b_N^a / g_N^a|^2 \tag{25}$$

with slot offsets and lengths (x_n^{off}, L_n), $n = 1, 2, ..N$ as variables and w_1, w_2, w_3 and w_4 being weighting factors related to the element excitations, input impedance matching, efficiency and resonance of the last slot, respectively. Since the first term involves a summation of $N - 1$ contributions, we typically use $w_1 = 1$ and $w2 = w3 = w_4 \approx N$. That is to ensure equitable consideration of each performance objective (i.e., the excitation of individual slots, input reflection coefficient, fraction of power absorbed in the load and normalized susceptance of the last slot) in the composition of the cost function.

As starting values, a moderate slot offset and resonant length for each slot would suffice. At the start of each iteration, the mutual coupling terms g_{mn}, h_n^{20} and h_n^{01} are computed with the most recent values for slot dimensions and kept constant during the ensuing optimization. To aid convergence, no mutual coupling is considered for the first iteration (i.e., $y_n^a = y_n^{\text{self}}$) and the mutual coupling terms are progressively scaled during the first half of the chosen number of iterations [11]. For the second half of the iterations, the full effects of mutual coupling are taken into consideration.

IV. VALIDATION

To demonstrate the validity of the design procedure, the 21-element array of [3] was redesigned at a frequency of 9.375 GHz. The element excitations listed in Table II were used. As in [3], an element spacing of $d = 0.389\lambda_{10} = 17.405$ mm and a slot width of $w = 1.6$ mm was selected, and the array was implemented in standard WR90 waveguide with a wall thickness of $t = 1.27$ mm. Weighting factors of $w_1 = 1$ and $w_2 = w_3 = w_4 = 25$ were used during the repeated minimization of (25) over a total of 16 iterations. With this choice of weights, the input VSWR and $P_{\text{L}}/P_{\text{in}}$

TABLE 3. Slot lengths and offsets of the 21-element traveling-wave array.

n	1	2	3	4	5	6	7
L_n (mm)	15.829	15.819	15.763	15.704	15.657	15.629	15.603
x_n^{off} (mm)	0.608	0.401	0.658	0.827	1.035	1.244	1.470
n	8	9	10	11	12	13	14
L_n (mm)	15.581	15.564	15.552	15.541	15.537	15.534	15.531
x_n^{off} (mm)	1.693	1.888	2.137	2.351	2.573	2.781	2.993
n	15	16	17	18	19	20	21
L_n (mm)	15.527	15.517	15.492	15.481	15.370	15.320	15.190
x_n^{off} (mm)	3.208	3.368	3.371	3.439	2.943	2.355	2.548

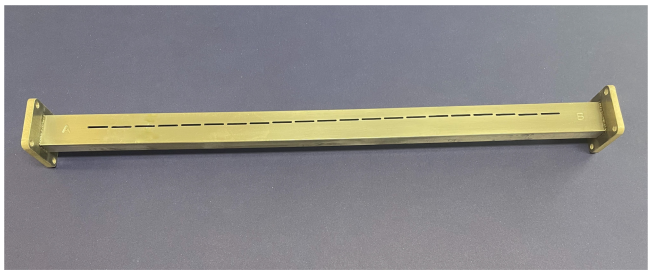

FIGURE 8. Prototype 21-element traveling-wave array.

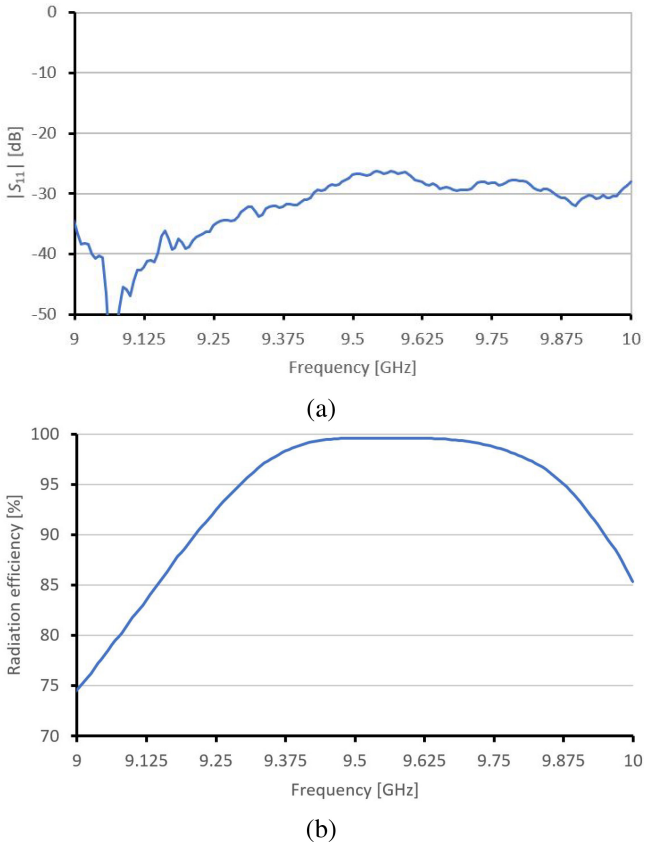

FIGURE 9. Measurements of (a) reflection coefficient and (b) radiation efficiency of the prototype array.

were computed to be 1.02 and 1.6% at 9.375 GHz. The final slot lengths and offsets are listed in Table III. The prototype array shown in Fig. 8 was manufactured using a 440 mm section of aluminium WR90 waveguide. The slots were CNC machined with 0.5 mm radius rounded corners.

Incidentally, using uniform weights (i.e., $w_1 = w_2 = w_3 = w_4 = 1$) in (25) results in an increase in VSWR and P_L/P_{in} to 1.09 and 4.5%, respectively. Our initial choice of $w2 = w3 = w_4 \approx N$ thus appears to be more appropriate.

The measured reflection coefficient of the prototype shown in Fig. 9(a) is below −25 dB for the entire frequency range of 9 to 10 GHz. For a traveling-wave array, low reflection over a range of frequencies does not necessarily imply high radiation efficiency, because some of the input power may be absorbed in the matched load termination. To assess the efficiency, measurements for the transmission coefficient S_{21} were also performed to obtain the fraction of power radiated by the array from

$$P_{\text{rad}}/P_{\text{in}} = 1 - |S_{11}|^2 - |S_{21}|^2. \tag{26}$$

The results depicted in Fig. 9(b) show that the array maintains 90% efficiency over a bandwidth of 8%. At the center of the band, less than 2% of the input power is absorbed in the matched load.

The H-plane radiation patterns were measured at sample frequencies and the array was also simulated in CST Microwave Studio. Fig. 10(a) shows the pattern at the design frequency of 9.375 GHz. It shows a well-developed main beam at the intended squint angle of $\theta_0 = 45°$ and the measured results meet the −30 dB sidelobe specification. At a frequency of 9.75 GHz, CST simulations predict elevated sidelobes close to the endfire direction, as depicted in Fig. 10(b). At this higher frequency, the reduced element spacing (relative to wavelength) is the cause of the emergence of a grating lobe. However, the secondary lobe is notably absent in the experimental results. This may be due to inadvertent shielding by the waveguide flanges at the end of waveguide section. Conversely, close agreement between the calculated and measured field in the vicinity of the main lobe is observed.

The simulated and measured gain of the prototype array is shown in Fig. 11. The measured gain is slightly lower than predicted, but the results are generally in good agreement. The reduction in gain at the higher end of the frequency range can be ascribed to increased power absorption in the matched load.

These results compare favorably to those reported in the literature for the same design example. In the original contribution [3], the innermost sidelobes of the radiation pattern at the design frequency of 9.375 GHz lie between −22 and −24 dB, and at angles around broadside, the SSL exceeds the −30 dB target by 5 dB. The input VSWR performance was very good over a 5% frequency band, but P_L/P_{in} was predicted to be 12.3%. In [4], [5], slot lengths and offsets of this array were perturbed to improve the array performance. Optimization was employed to minimize

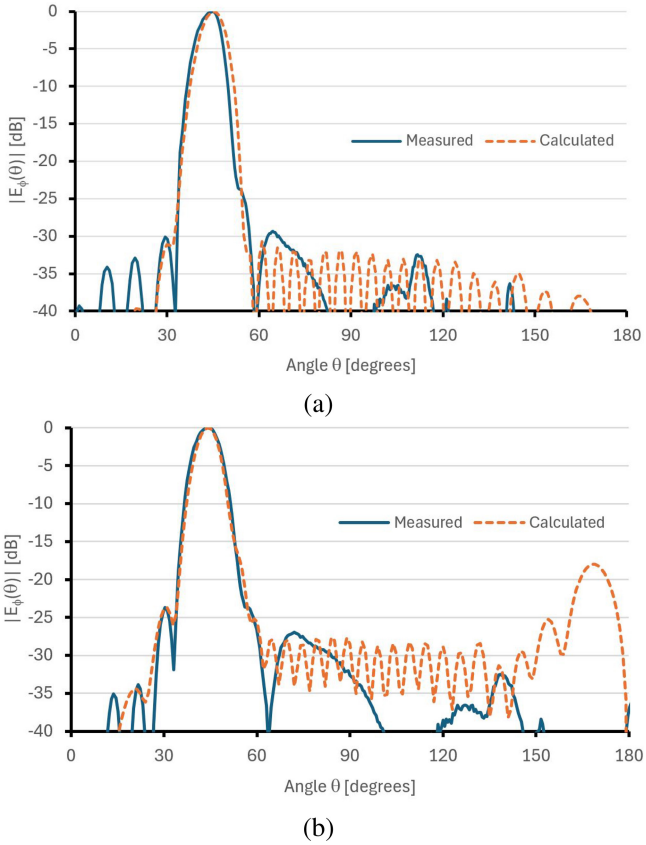

FIGURE 10. Calculated and measured H-plane radiation pattern of the prototype array at frequencies of (a) 9.375 GHz (design frequency) and (b) 9.75 GHz.

either the (a) VSWR and P_L/P_{in}, (b) frequency bandwidth, or (c) SSL. For case (a), P_L/P_{in} was reduced to 2.1% at 9.375 GHz, but that was achieved at the expense of an SSL of −22.1 dB. In case (b) with a bandwidth of 5%, theoretical results show an SSL better than −21.9 dB and P_L/P_{in} lower than 6.2% within the band. For case (c), the SSL was reduced to a maximum of −25.2 dB, but power in the load increased to 4.6%. Note that although optimization was specifically applied to reduce the sidelobes, the initial design target of −30 dB was not met. This underscores the value of our proposed approach where element excitations are adjusted in accordance with SLL specifications before slot dimensions are computed.

V. CONCLUSION

The proposed design approach for traveling-wave slot arrays thus comprises two distinct steps. During the first step, the element excitations are adjusted to account for elevated sidelobes caused by the element pattern. The second phase involves the calculation of the physical slot dimensions using an iterative process with repeated optimization of slot dimensions. This method is capable of producing the desired radiation characteristics while achieving impedance matching and high levels of antenna efficiency.

The procedure was validated by designing and constructing a 21-element array in standard WG90 waveguide.

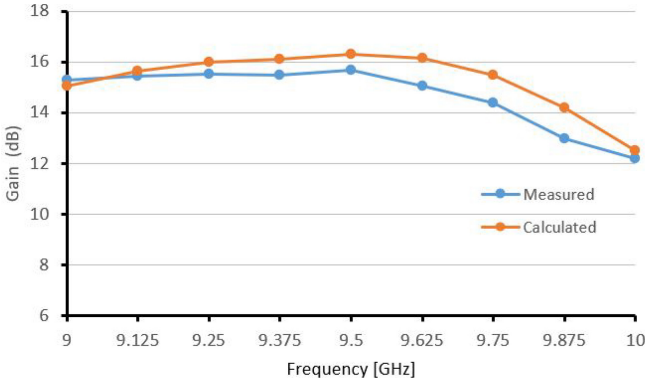

FIGURE 11. Calculated and measured gain of the prototype array versus frequency.

The array satisfied the specifications, and good agreement between simulated and measured results were observed.

This approach is highly efficient. Full-wave analysis is only employed during the initial generation of a database for the self-admittance $y^{self}(x^{off}, L)$ over a range of typical offsets and lengths. This can be accomplished with relative ease and speed. Assuming a fixed design frequency and waveguide dimensions, this task only needs to be performed once. Full-wave analysis does not form part of the repeated optimization steps of the design stage. The optimization objective function comprises analytical expressions, thus facilitating rapid computation. This formulation is suitable for implementation on a regular personal computer, and with slot data readily available, execution time can typically be measured in minutes or even seconds.

REFERENCES

[1] A. J. Sangster, "Conventional waveguide-fed travelling-wave slot arrays," in *Compact Slot Array Antennas for Wireless Communications. Signals and Communication Technology*, Cham, Switzerland: Springer, 2019. [Online]. Available: http://dx.doi.org/10.1007/978-3-030-01753-8_7

[2] J. Hirokawa and M. Zhang, "Waveguide slot array antennas," in *Handbook of Antenna Technologies*, Z. Chen, Ed. Singapore: Springer, 2015. [Online]. Available: http://dx.doi.org/10.1007/978-981-4560-75-7_51-1

[3] R. S. Elliott, "On the design of traveling-wave-fed longitudinal shunt slot arrays," *IEEE Trans. Antennas Propag.*, vol. 27, no. 5, pp. 717–720, Sep. 1979, doi: 10.1109/TAP.1979.1142166.

[4] A. Jensen and S. R. Rengarajan, "Genetic algorithm optimization of a traveling wave array of longitudinal slots in a rectangular waveguide," *ACES J.*, vol. 21, no. 2, pp. 337–341, Apr. 2013.

[5] L. Josefsson and S. R. Rengarajan, *Slotted Waveguide Array Antennas: Theory, Analysis and Design*, London, U.K.: SciTech Publ., 2018. [Online]. Available: http://dx.doi.org/10.1049/SBEW517E

[6] S. R. Rengarajan, "Genetic algorithm optimization of traveling wave slot arrays using full wave method of moments analysis," in *Proc. 32nd URSI Gener. Assembly Sci. Symp.*, 2017, p. 1.

[7] C. A. Balanis, *Antenna Theory: Analysis and Design*. New York, NY, USA: Wiley, 1997, p. 302.

[8] R. S. Elliott, "An improved design procedure for small arrays of shunt slots," *IEEE Trans. Antennas Propag.*, vol. 31, no. 1, pp. 48–53, Jan. 1983, doi: 10.1109/TAP.1983.1143002.

[9] J. C. Coetzee, J. Joubert, and D. A. McNamara, "Off-center-frequency analysis of a complete planar slotted-waveguide array consisting of subarrays," *IEEE Trans. Antennas Propag.*, vol. 48, no. 11, pp. 1746–1755, Nov. 2000, doi: 10.1109/8.900233.

[10] J. C. Coetzee and S. Sheel, "Waveguide slot array design with compensation for higher order mode coupling between inclined coupling slots and neighboring radiating slots," *IEEE Trans. Antennas Propag.*, vol. 67, no. 1, pp. 378–389, Jan. 2019, doi: 10.1109/TAP.2018.2876118.

[11] J. C. Coetzee and S. Sheel, "Precision design of slot arrays in reduced-height, dielectric-filled or substrate-integrated waveguide using the full T-network equivalent circuit for array elements," *Electromagnetics*, vol. 42, no. 4, pp. 241–254, Aug. 2022, doi: 10.1080/02726343.2022.2110016.

[12] R. S. Elliott and W. O'Loughlin, "The design of slot arrays including internal mutual coupling," *IEEE Trans. Antennas Propag.*, vol. 34, no. 9, pp. 1149–1154, Sep. 1986, doi: 10.1109/TAP.1986.1143947.

JACOB C. COETZEE (Senior Member, IEEE) was born in Pretoria, South Africa, in 1964. He received the B.Eng. (cum laude), M.Eng. (cum laude), and Ph.D. degrees in electronic engineering from the University of Pretoria, Pretoria, South Africa, in 1987, 1989, and 1994, respectively. He was with the University of Pretoria from 1994 to 1997 and the National University of Singapore, Singapore, from 1998 to 2007. He joined the Queensland University of Technology, Brisbane, QLD, Australia, in 2008. His research interests include analysis and synthesis of microwave circuits, antenna arrays, and smart antennas.